VI International Conference on Computational Methods in Marine Engineering
MARINE 2015
F. Salvatore, R. Broglia and R. Muscari (Eds)

IMPACT OF WATER DEPTH ON ROWING FAIRNESS

EDIE MIGLIO, NICOLA PAROLINI AND MATTEO PISCHIUTTA

MOX - Dipartimento di Matematica
Politecnico di Milano
Piazza Leonardo da Vinci 32, 20133 Milano, Italy

Key words: Shallow Water, Free-Surface Flows, Rowing

Abstract. Among the regulations of the Fédération Internationale des Sociétés d'Aviron (FISA) for international events, one states that a rowing course should have a minimum depth of 3.5 metres. In this work, we analyse the effect of the water depth on rowing basin recirculation and boat performance in order to assess at which extent this rule limitation is supported by physical evidence.

1 INTRODUCTION

The reduction of the rowing course depth would affect the wind induced flow in the course and also the boat hydrodynamics. On the one hand, the wind blowing on a enclosed water basin creates a downwind lowering and a upwind rise of the free surface. This surface configuration induces a pressure gradient which in turn generates a complex three dimensional flow pattern mainly characterized by a bottom flow in the opposite direction with respect to the blowing wind. The conservation of mass ensure however that this flow pattern has zero net mass flux in any vertical plane, so that the recirculation depends strongly on basin shape and bathymetry. In this work we quantify the impact of water depth on the wind-induced superficial water currents which can produce unfair race conditions.
On the other hand, a hull moving through water generates a wave pattern moving with the hull and a region of perturbed flow extending as a wake behind the hull. Two different kinds of forces constitute the components of the resistance [1]: the *frictional drag*, due the tangential shear force, and the *pressure drag*, due to normal pressure forces. The frictional drag arises purely because of the viscosity, but the pressure drag is due in part to the shape of the hull (*form resistance*), in part to the formation of boundary layer (*viscous pressure resistance*) and in part to the generation of waves (*wave making resistance*) [2]. In this work we quantify the impact of water depth on the components of resistance of Olympic rowing hull; moreover we analyse the effect of water depth on wave pattern, identifying at which conditions the fairness of the competition would be compromised.

2 MATHEMATICAL AND NUMERICAL MODELS

In order to investigate the impact of the basin depth on the fairness of a rowing race, we discuss in this work two different kinds of analysis that can be carried out. On one side, at the basin scale, the effect of the water depth on the flow recirculation in the rowing course is investigated solving the 3D shallow water equations; on the other hand, the influence of the water depth on the local free-surface hydrodynamics around a rowing boat is simulated solving the 3D Reynolds Averaged Navier-Stokes (RANS) equations for a two-phase flow.

2.1 Course recirculation model

The course recirculation has been simulated using TELEMAC-3D [3], which solves the Navier-Stokes equations with a free surface boundary condition on a layered finite-element mesh. TELEMAC-3D is a well assessed numerical tool which accounts for the main physical phenomena which are relevant in this kind of free-surface flows, including friction on the course bed and lateral boundaries, wind stress on the free surface and turbulence. We refer to [3] for a detailed description of the mathematical model and numerical methods adopted in TELEMAC-3D. Here, the main features of the solver are briefly recalled.

3D shallow-water model In the 3D shallow-water approach adopted in TELEMAC-3D the hydrostatic pressure hypothesis is considered and the pressure is defined as $p(x,y,z,t) = \rho g(Z_s - z)$, where p is the pressure, ρ is water density, g is the gravitational acceleration and $Z_s = Z_s(x,y,t)$ is the elevation of the free-surface. Under this hypothesis and neglecting the diffusive and inertial terms in the equation for the vertical velocity, the three-dimensional Navier-Stokes equations can be rewritten in the following shallow-water formulation:

$$
\begin{aligned}
&\frac{\partial U}{\partial x} + \frac{\partial V}{\partial y} + \frac{\partial W}{\partial z} = 0,\\
&\frac{\partial U}{\partial t} + U\frac{\partial U}{\partial x} + V\frac{\partial U}{\partial y} + W\frac{\partial U}{\partial z} = -g\frac{\partial Z_s}{\partial x} + \nu\nabla^2 U,\\
&\frac{\partial V}{\partial t} + U\frac{\partial V}{\partial x} + V\frac{\partial V}{\partial y} + W\frac{\partial V}{\partial z} = -g\frac{\partial Z_s}{\partial y} + \nu\nabla^2 V,
\end{aligned}
$$

where $\mathbf{U} = (U,V,W)$ is the velocity field and ν is the effective viscosity. The fractional step scheme implemented in TELEMAC-3D requires to solve, at each time step, the following problems:

1. *Advection step:* the method of characteristics is used to compute a first intermediate velocity solving for the advection terms;

2. *Diffusion step:* the intermediate velocity is corrected accounting for the diffusion and source terms in the momentum equations;

3. *Pressure-continuity step:* the water depth is computed from the vertical integration of the continuity and the momentum equations only including the pressure-continuity terms, by solving the following system

$$\begin{aligned}
&\frac{\partial h}{\partial t} + \frac{\partial (uh)}{\partial x} + \frac{\partial (vh)}{\partial y} = 0,\\
&\frac{\partial u}{\partial t} = -g\frac{\partial Z_s}{\partial x},\\
&\frac{\partial v}{\partial t} = -g\frac{\partial Z_s}{\partial y},
\end{aligned}$$

where u and v are the vertically integrated x and y velocities and h is the water depth $h(x,y,t) = Z_s(x,y,t) - Z_f(x,y)$, with $Z_f(x,y)$ denoting the basin bathymetry.

Turbulence modelling A common practice in numerical computation of environmental free surface flows consists in separating the vertical and horizontal turbulence models. This is justified by the difference between the horizontal ($\sim$ 1 Km) and vertical ($\sim$ 1 m) scales. That involves defining horizontal as well as vertical turbulent viscosities rather than a single viscosity. In wind induced water current, the vertical turbulent viscosity plays the most relevant role. The vertical turbulent viscosity is defined in TELEMAC-3D based on the mixing length hypothesis using the Tsanis model [4].

Bottom friction The effect of bottom friction is taken into account as a boundary condition for the momentum equation and reads:

$$\nu \frac{\partial \mathbf{U_H}}{\partial \mathbf{n}} = -\frac{C}{2} |\mathbf{U_H}| \, \mathbf{U_H},$$

where $\mathbf{U_H} = (U, V)$ is the horizontal velocity at the bottom and the coefficient C is given by the Nikuradse formula: $C = 7.83 \ln\left(12\frac{h}{k_s}\right)$, where k_s is the roughness of the bottom. Usually $k_s = 3.5\, D_{84}$, where D_{84} is the average diameter of the 84^{th} largest percentile of the grains of the bed material. For the simulations presented in this work the value $k_s = 1$ cm (which correspond to a coarse gravel bed) has been considered.

Wind force The force exerted by the wind on the free-surface is modelled as a stress boundary condition on the free-surface in a similar way as for the bottom friction, namely

$$\nu \frac{\partial \mathbf{U_H}}{\partial \mathbf{n}} = \frac{\rho_{\text{a}}}{\rho_{\text{w}}} a_{\text{wind}} |\mathbf{U}_{\text{wind}}| \, \mathbf{U}_{\text{wind}},$$

where ρ_{a} and ρ_{w} are the air and water densities, respectively, $\mathbf{U}_{\text{wind}} = (U_{\text{wind}}, V_{\text{wind}})$ is the 2D wind velocity field and a_{wind} is the wind forcing coefficient given by Flather [5].

2.2 Boat hydrodynamic model

For the simulation of the free-surface flow around the rowing boat, the full 3D RANS equations are solved. The Volume-Of-Fluid (VOF) method has been adopted to capture the free-surface using the approach implemented in the `interFoam` solver family available in the OpenFOAM finite-volume library [6]. Although it is possible to simulate the complete dynamics of the rowing boat [7, 8, 9], in this work the analysis is limited to the evaluation of forces and wave patterns for steady state conditions. A dynamic mesh strategy is used to move vertically the hull in order to ensure that, at steady state, the hydrodynamic vertical equilibrium between the lift force and the boat displacement is reached.
The computational mesh is generated using the `snappyHexMesh` utility which starts from a *stl* description of the hull geometry and builds (with a semi-automatic procedure) a 3D hexa-core mesh with boundary layer refinement. The simulations were obtained with affordable computational costs using the `LTSInterFoam` solver suitably modified to account for the mesh motion required to reach the hydrodynamic equilibrium.

3 NUMERICAL RESULTS

In this section we present the results of the numerical simulations of the rowing course recirculation and of the local free-surface flow around the boat.

3.1 Simulations of rowing course recirculation

We have analysed the wind induced hydrodynamics in Eton Dorney rowing course, used as the 2012 Summer Olympic venue for rowing and canoe sprint. The lake consists in a main basin 2200 m long, 147 m wide and with minimum depth of 3.5 m, with 8 lanes each 13.5 m wide, and a parallel warm-up channel 2.5 m deep and up to 5 lanes wide. According to the informations provided by the MetOffice before the Olympic Games [10], in the summer the prevailing wind is from the west, with average speed of 2.8 m/s at 10 m height. The geometry of the lake has been digitalised through the OpenStreetMap Editing API, which allows to extract geo-data from the OpenStreetMap database. For the sake of simplicity we neglect the depth differences between the two zones of the lake and create an artificial bathymetry with the explicit functional form:

$$Z_f(x, y) = \max(-D, -\gamma\, d(x, y)),$$

where D is the maximum depth of the lake, $\gamma = 0.25$ is the slope of the banks and $d(x, y)$ is the distance from the lake boundary, see Fig.1(a).
The two dimensional mesh for the finite elements computation consists in a Delaunay triangulation with highest resolution at the lake boundaries, that are the shallower zones of the domain. Far from the lake boundaries the mesh size is constant. After a mesh convergence analysis, the size of the mesh τ used in this study varies from $\tau_{\min} = 0.5\, m$

at the lake boundaries to $\tau_{\max} = 5\,m$ in the deepest region, see Fig.1(b).

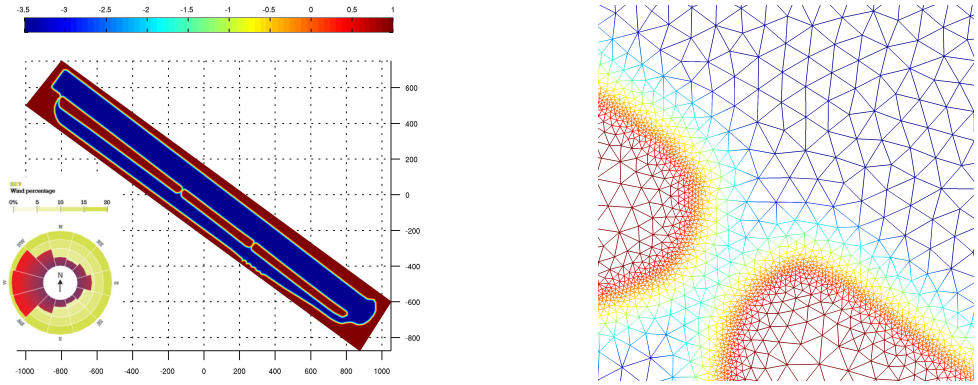

(a) (b)

Figure 1: Eton Dorney rowing course; wind rose, geometry and bathymetry (a); detail of the computational mesh between two islands (b).

We consider the depths $D = 3.5\,m$ (the real one for the main basin) and a hypothetical shallower one $D = 2\,m$, and analyse the differences on the wind induced hydrodynamic in the cases of a constant wind blowing from west at the speed of 2, 10 and 20 m/s. Such wind direction induces a superficial water current with the qualitative behaviour depicted in Fig.2(a): we can see that the north-eastern half of the main lake encounters a current almost aligned with the forcing wind, and hence a positive velocity in race direction, while the south-western half must even face a counter-current near the lake boundary. This qualitative recirculation pattern is almost independent from wind velocity and water depth, and hence is a common feature for all the cases considered.

To quantify the advantages for the lanes in the left side of the course we choose to extract, from the obtained three dimensional velocity fields, the velocity component aligned with rowing direction averaged in the upper 10 cm of water; this is an indicator of the local drag encountered by each crew. The results for the wind blowing at 10 m/s are depicted as example in Fig.2(b)-(c); we can see that for both course depths considered there are important differences in the stream velocity among the eight lanes of the course. The first lane crew has the greatest advantage, being dragged by the greatest stream velocity, then the others lanes crews encounter a lower stream velocity, which becomes negative for the most part of the course in the eighth lane.

In Table 1 we average the local superficial velocity along all the course; the obtained values are an indicator of the global drag encountered by the crews. We observe that:

1. the average stream velocity in the 1$^{\text{st}}$ lane is independent from water depth and is proportional to wind intensity ($\simeq 1.28\%$);

2. for every wind intensity, the 2 m course depth induces a velocity difference from 1st to 6th lane lower than in the 3.5 m course depth;

3. for every wind intensity, the velocity difference from 2nd to 7th lane is almost independent from course depth;

4. the counter-current velocity in the 8th lane is higher in the 2 m course depth case.

Wind velocity and water depth	Mean stream velocity in rowing direction [m/s] in lane number:							
	1	2	3	4	5	6	7	8
2 m/s - 2.0 m	0.0253	0.0218	0.0188	0.0157	0.0123	0.0083	0.0035	-0.0026
2 m/s - 3.5 m	0.0254	0.0214	0.0177	0.0141	0.0105	0.0067	0.0030	-0.0009
10 m/s - 2.0 m	0.1276	0.1099	0.0946	0.0787	0.0617	0.0412	0.0171	-0.0133
10 m/s - 3.5 m	0.1275	0.1072	0.0889	0.0706	0.0526	0.0338	0.0153	-0.0047
20 m/s - 2.0 m	0.2561	0.2205	0.1897	0.1578	0.1236	0.0825	0.0345	-0.0265
20 m/s - 3.5 m	0.2552	0.2146	0.1779	0.1413	0.1053	0.0677	0.0308	-0.0092

Table 1: Average flow velocities in race direction in the upper water layer for each rowing line.

With those considerations in mind, we can conclude that, for all the wind intensities considered, the course depth of 2 m does not affect the fairness of the competition more than the course depth of 3.5 m.

3.2 Simulations of free-surface boat hydrodynamics

We simulated the flow around three different classes of rowing boats (2, 4 and 8 rowers crews) at four different depths (3.5, 3, 2.5 and 2 m). The displacements of the 2-, 4- and 8-rowers hulls are 165 kg, 431 kg and 877 kg, respectively. The simulations for the three rowing classes were run at constant speed of 5 m/s, 5.75 m/s and 6.5 m/s, respectively.

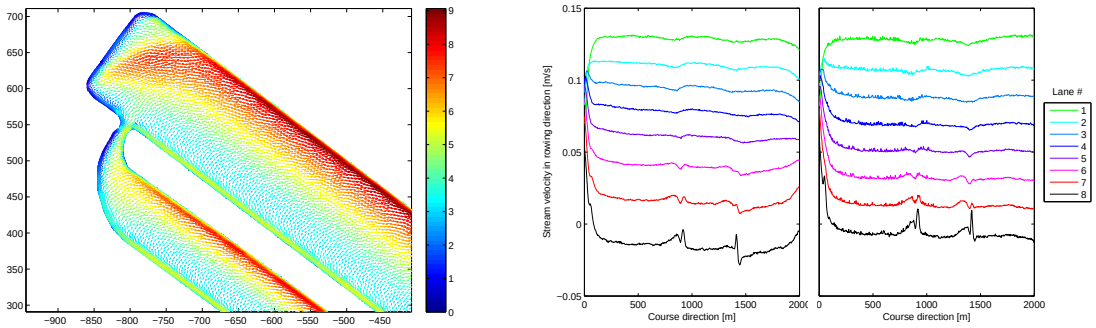

(a) Velocity vectors (b) Depth: 2 m (c) Depth: 3.5 m

Figure 2: Results of the mean velocity in the upper 10 cm of water: superficial current induced in the starting zone (a) and component aligned with rowing direction in all the lanes in 2 m (b) and 3.5 m (c) cases. Wind speed is 10 m/s.

Forces There are different factors that may affect the resistance in shallow water: firstly, the *viscous* drag may change due to the acceleration induced by the flow confinement between the hull and the bottom of the channel; secondly, the water depth may also have an effect on the draft of the hull (and its wetted surface) which again would impact on the *viscous* resistance. Finally, it is well known that the waves produced in shallow water have a larger amplitude than in deep water. Hence, the energy required to produce these waves is larger. This effect increases the *pressure* wave resistance.
In Table 2 we report the resulting viscous and pressure drag obtained in our simulations. First of all we observe that, for every boat and depth considered, the viscous effect is the main component of the rowing boat resistance; considering all cases, almost the 92% of the total resistance is due to viscous drag. Then in Table 3 we report the variations (absolute and relative) of the forces with respect to the 3.5 m conditions. We observe that at every depth considered, the viscous drag is not much affected by water depth; its maximum variation with respect to 3.5 m conditions, is of the order of 1%.

	Viscous drag $[Kg]$				Pressure drag: $[Kg]$				Total drag: $[Kg]$		
Depth:	2	4	8		2	4	8		2	4	8
$3.5m$	11.56 (95.07%)	27.99 (92.90%)	54.83 (94.55%)	+	0.60 (4.93%)	2.14 (7.10%)	3.16 (5.45%)	=	12.16 (100%)	30.13 (100%)	57.99 (100%)
$3.0m$	11.55 (92.47%)	27.93 (93.54%)	54.80 (94.76%)		0.94 (7.53%)	1.93 (6.46%)	3.03 (5.24%)		12.49 (100%)	29.86 (100%)	57.83 (100%)
$2.5m$	11.47 (93.25%)	27.91 (93.85%)	54.79 (94.94%)		0.83 (6.75%)	1.83 (6.15%)	2.92 (5.06%)		12.30 (100%)	29.74 (100%)	57.71 (100%)
$2.0m$	11.45 (93.70%)	27.84 (94.09%)	54.72 (95.03%)		0.77 (6.30%)	1.75 (5.91%)	2.86 (4.97%)		12.22 (100%)	29.59 (100%)	57.58 (100%)

Table 2: Resulting drag for all the boats and the depth considered, with relative contribution to total drag in brackets.

	Viscous drag $[Kg]$				Pressure drag: $[Kg]$				Total drag: $[Kg]$		
Depth:	2	4	8		2	4	8		2	4	8
$3.5m$	0.00 (0.00%)	0.00 (0.00%)	0.00 (0.00%)	+	0.00 (0.00%)	0.00 (0.00%)	0.00 (0.00%)	=	0.00 (0.00%)	0.00 (0.00%)	0.00 (0.00%)
$3.0m$	-0.01 (-0.08%)	-0.06 (-0.20%)	-0.03 (-0.05%)		0.34 (2.80%)	-0.21 (-0.70%)	-0.13 (-0.22%)		0.33 (2.71%)	-0.27 (-0.90%)	-0.16 (-0.28%)
$2.5m$	-0.09 (-0.74%)	-0.08 (-0.27%)	-0.04 (-0.07%)		0.23 (1.89%)	-0.31 (-1.03%)	-0.24 (-0.41%)		0.14 (1.15%)	-0.39 (-1.29%)	-0.28 (-0.48%)
$2.0m$	-0.11 (-0.90%)	-0.15 (-0.50%)	-0.11 (-0.19%)		0.17 (1.40%)	-0.39 (-1.29%)	-0.30 (-0.52%)		0.06 (0.49%)	-0.54 (-1.79%)	-0.41 (-0.71%)

Table 3: Differences of drag with respect to the 3.5 m depth conditions. In brackets, the relative increment with respect to the total drag force at 3.5 m depth.

Analysing our results, we first observe that the region where the flow is perturbed by the presence of the hull (*i.e.* the *boundary layer*) extends up to a distance of 0.1 m from the hull, and that the velocity profiles in the boundary layer are almost identical for all the

depths considered. Under this distance from the hull, the flow is unperturbed and hence the effect of the reduced depth, at least for the range of depth that we are considering, has no consequences on the velocity profiles. Secondly, as our simulations run with a dynamic mesh solver, we can analyse the drafts of the boats at the hydrodynamic equilibrium. Our results reports that decreasing the water depth induces a decrease of the draft of the hull of the order of 1 mm from the deeper to the shallower cases. The decrease of the draft reduces the wetted surface of the hull, which in turn explains the decrease of the viscous drag that we noticed in Table 3.
On the other side, as expected, the pressure drag is greatly affected by depth effects. In fact, part of the pressure drag is due to wave making resistance, and the wave pattern strongly depends on water depth, as it will be discussed in the next session. However, we cannot isolate in our results the contribution of the wave making resistance from the form and viscous pressure resistance.

Wave patterns The wave pattern in shallow water depends on the flow regime. The dimensionless depth Froude number $\mathrm{Fr}_h = \frac{V}{\sqrt{gh}}$ is the main parameter used to describe the flow regime, where V is the boat speed, g is gravity acceleration and h is water depth. When $\mathrm{Fr}_h < 1$, the regime is called *sub-critical* and the wave pattern consists of divergent and transverse waves. The transverse waves are perpendicular to the ship axis and follow the ship at the same speed V, while the enveloping wedge of the divergent system intersects the sailing line at a fixed angle of $\arcsin(1/3) \simeq 19.5°$, the so called Kelvin angle. As Fr_h increases, the wave pattern changes. The angle of the enveloping wedge widens, until at the critical $\mathrm{Fr}_h = 1.0$ it is perpendicular to the ship's track. In fact, at the critical regime, the velocity of the boat and waves are equal to $\sqrt{gh}$. In linear theory the energy does not disperse back along the transverse wave train, as in sub-critical conditions. Consequently a significant proportion of the power of the boat is converted into wave energy in a few wave fronts nearly perpendicular to the ship axis, whilst the transverse system is ultimately lost with only the divergent system remaining. At higher $\mathrm{Fr}_h > 1.0$, the waves are non-dispersive since all wavelengths travel at same speed $\sqrt{gh}$. The stationary waves cannot travel in the direction of the boat as the water depth limits their speed. Therefore the wave fronts subtend an angle of θ to the course of the craft so that $\sqrt{gh} = V\cos\theta$, that is $\theta = \arccos(1/\mathrm{Fr}_h)$. Consequently all the wave components radiate out in lines from the ship in a V-like formation.
In Fig.4 we report all the wave patterns obtained in our study. Considering Fig.4 (subfigures a,b,c,d), we first notice that the 2-rowers boat, travelling at 5 m/s, at depth of 3.5 m is in the sub-critical regime with $\mathrm{Fr}_h = 0.85$; we observe the classical wave pattern with both transverse and diverging wave. Decreasing the water depth at 3.0 m results in a $\mathrm{Fr}_h = 0.92$; the regime is still sub-critical, we still observe diverging dispersive waves but the transverse waves have disappeared. The interesting phenomena appears at 2.5 m depth: here $\mathrm{Fr}_h = 1.01$ and the regime is essentially critical. We observe that the bow wave is almost perpendicular to the ship axis and in the wake regions appears a depression

of the free surface. This is due to the fact that both the ship and the wave travels at same speed, hence a constructive interference between wave generation and propagation establishes. At 2.0 m depth, $\mathrm{Fr}_h = 1.13$ and the regime is super-critical; the diverging waves are no more dispersive and the crests/trough lines have almost the same inclination. Consider now Fig.4 (subfigures e,f,g,h), that is the 4 rowers boat, travelling at the higher speed of 5.75 m/s. At this speed, at the 3.5 m depth, the $\mathrm{Fr}_h = 0.98$ means that the regime is essentially critical. The same considerations done for the 2 rowers hull at 2.5 m depth hold. At the reduced depths, the regime is super critical and once again the crests/trough lines of the waves have the same Kelvin angle θ which decreases with depth through the relation $\theta = \arccos(1/\mathrm{Fr}_h)$.
Finally, considering Fig.4 (subfigures i,j,k,l), *i.e.* the 8 rowers boat which travels at 6.5 m/s, we can observe that the regime is super-critical at any depth, Fr_h going from 1.11 at 3.5 m to 1.35 at 2.0 m. Once again, the wave pattern consists in diverging non-dispersive waves with Kelvin angle decreasing with depth.
It is well known in the literature [1] that as the speed approaches the critical speed a significant amplification of wave resistance occurs, while at speeds greater than critical the wave resistance reduces again. In Fig.3 we show the trend of the pressure drag with respect to depth Froude number: the theoretical decreasing of pressure drag for $\mathrm{Fr}_h > 1$ is reproduced in our simulations and, as expected, the peaks are located around $\mathrm{Fr}_h = 1$.

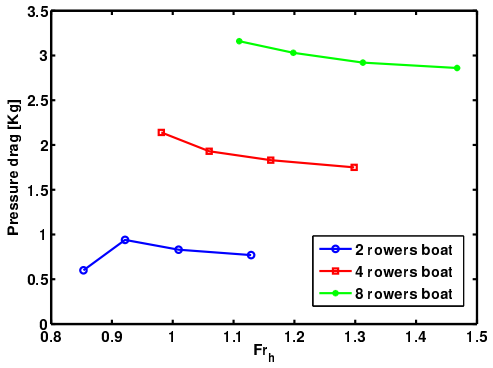

Figure 3: Depth Froude number vs pressure drag.

Wave interference among lanes Another interesting question that we can answer based on our analysis is: how the waves generated by the leading boat propagate in adjacent lines? The answer is in Fig.5, where we plot the wave height at the distance of 15 m from the center line of the boats.
Looking at the 2-rowers boat results in Fig.5(a), the first interesting consideration is that in sub-critical conditions (3.5 and 3.0 m, red and green dots), the crest of the bow wave dissipate before reaching the adjacent line. Hence in sub-critical conditions the adjacent line first see the mid-boat wave through; *e.g.* at a depth of 3.0 m there is a wave through

of 6 mm situated 16 m behind the bow of the boat generating waves. Another interesting consideration have to be made for the critical case at depth 2.5 m; as we have seen, in critical conditions the bow wave is perpendicular to ship axis, then we can see (blue dots) that in adjacent line the wave height is > 0 even before the point $x = 0$ that is the coordinate of the bow of the boat generating the waves. Finally, in the super-critical regime (violet line) the waves are not dispersive and the crest line of the bow wave do reach the adjacent line. In particular, the wave height in the adjacent line for the depth of 2.0 m shows a crest of 3 mm situated 13 m behind the bow of the leading boat.
Similar considerations can be made for the 4-rowers boat, see Fig.5(b). The red wave line, relative to the critical case at 3.5 m, shows again a free surface elevation greater than 0 even before the position $x = 0$ and a crest of 5 mm situated 7 m behind the bow of the leading boat. Decreasing the water depth, hence falling in the super-critical conditions, leads to a narrower Kelvin angle. This results in a wave crest position in adjacent line which is always of the same order of magnitude ($\simeq 5$ mm) but located 12.5, 15.5 and 18.5 m behind the bow of leading boat for the depths of 3.0, 2.5 and 2.0 m respectively.
Finally, for the 8-rowers boat, in Fig.5(c) we observe that, since the regime is always super-critical, the wave pattern in adjacent line shows a similar trend for all depth considered. Always for the same reason (narrowing of the Kelvin angle with decreasing depth), the first wave crest in adjacent line is situated at 15.5, 18, 20.5 and 23.7 m behind the bow of the leading boat for the 3.5, 3.0, 2.5 and 2.0 m depths respectively.

4 Conclusions

We have quantified the effect of depth on the superficial wind-induced current, for the wind direction and intensities considered, showing that a reduced course depth of 2 m does not affect the fairness of the competition more than the course depth of 3.5 m. We have performed a complete analysis of the different components of resistance and the wave pattern at different boat speeds and course depths. We showed that the viscous resistance is poorly affected by water depth, whilst the pressure resistance, in particular its component related to the wave making resistance, is greatly affected by water depth. In any case, as the main component of the total resistance is the viscous one ($> 92.5\%$), the relative variations with respect to the total resistance at 3.5 m depth are limited in the range of $[-1.8\%, +2.7\%]$, see Table 3. However, these differences are equal for all the boats, so the fairness of the race is not affected by the variations in resistance itself.
On the other side, what can really affect the fairness of the course is the wave interference among adjacent lanes. We showed that the bow wave generated by in one lane could propagate almost perpendicularly if the velocity of the hull is near the critical speed. Moreover, to avoid this phenomena we showed that increasing the Froude number above its critical value leads to a narrowing of the Kelvin angle, and hence the bow wave arrives farther in the adjacent lane.
With these considerations in mind, we recall that the critical speeds for the 3.5, 3.0 and 2.5 m depths are equal to 5.86, 5.42 and 4.95 m/s respectively. Those speeds are abso-

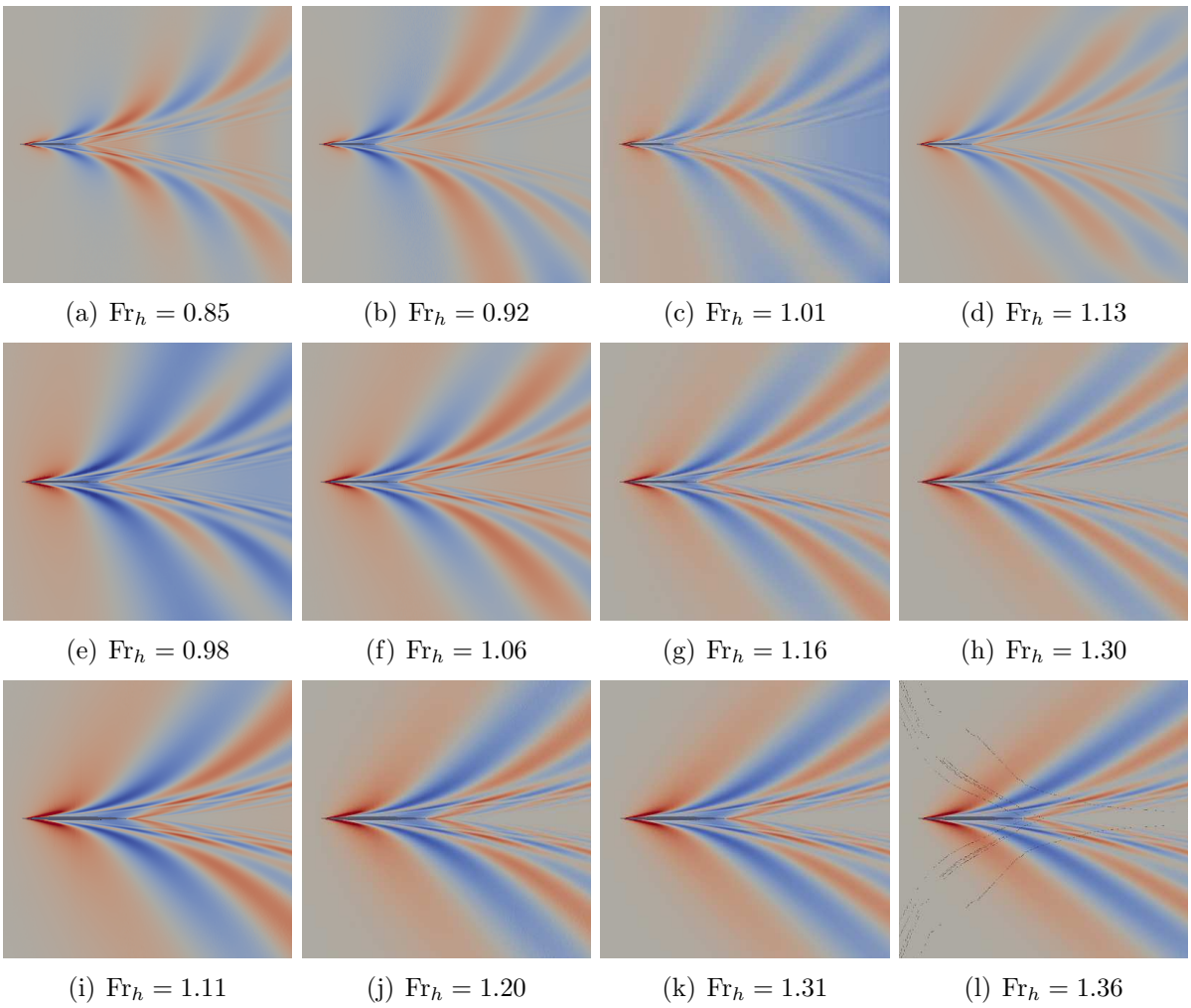

(a) $\mathrm{Fr}_h = 0.85$ (b) $\mathrm{Fr}_h = 0.92$ (c) $\mathrm{Fr}_h = 1.01$ (d) $\mathrm{Fr}_h = 1.13$

(e) $\mathrm{Fr}_h = 0.98$ (f) $\mathrm{Fr}_h = 1.06$ (g) $\mathrm{Fr}_h = 1.16$ (h) $\mathrm{Fr}_h = 1.30$

(i) $\mathrm{Fr}_h = 1.11$ (j) $\mathrm{Fr}_h = 1.20$ (k) $\mathrm{Fr}_h = 1.31$ (l) $\mathrm{Fr}_h = 1.36$

Figure 4: Wave patterns. Top row is the 2 boat, center row the 4 boat, bottom row the 8 boat. From left to right the water depth decreases from 3.5 to 2 m.

lutely within the range of speeds of the rowing boats considered (*e.g.*, the 2 and 4 rowers boats travels at critical conditions at 2.5 m and 3.5 m respectively) hence those depths should be avoided to limit the interferences of the waves generated by the hull.
The best choice seems to be the depth of 2.0 m, where the critical speed is equal to 4.3 m/s, which is lower than all the speeds considered in our study.

Acknowledgements

This research has been supported by the World Rowing Federation (FISA, Fédération Internationale des Sociétés d'Aviron). The authors would like to thank Matt Smith for the fruitful discussions.

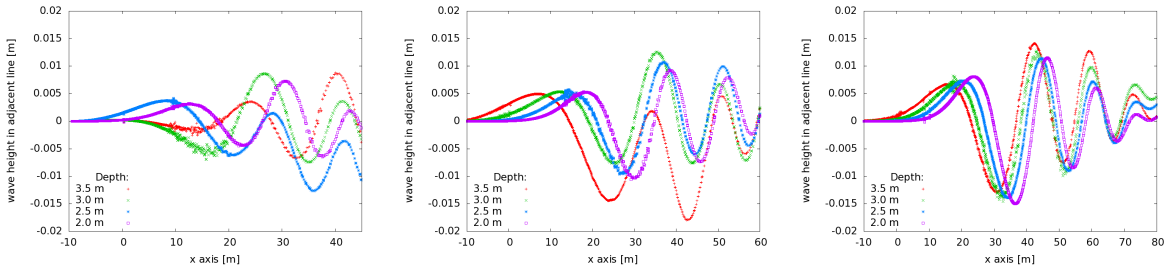

(a) 2-rowers boat (b) 4-rowers boat (c) 8-rowers boat

Figure 5: Wave height in adjacent line for the 2, 4 and 8 rowers boat. The bow of the boat generating the waves is at position $x = 0$.

REFERENCES

[1] Molland, A.F., Turnock, S.R. and Hudson, D.A. *Ship resistance and propulsion: practical estimation of propulsive power*. Cambridge University Press, (2011).

[2] Havelock, T. The wave-making resistance of ships: a theoretical and practical analysis. *Proc. of the Royal Society of London. Series A*, (1909) **82**(554):276-300.

[3] Hervouet. J.M. *Hydrodynamics of Free Surface Flows: Modelling with the finite element method*. John Wiley & Sons, (2007).

[4] Tsanis, I.K. Simulation of wind-induced water currents. *J. Hydraul. Eng.*, (1989) **115**(8):1113-1134.

[5] Flather, R.A. *Results from surge prediction model of the North-West European continental shelf for April, November, and December 1973*. Institute of Oceanography, (1976) Report n° 24

[6] OpenCFD (2014). *OpenFOAM - The Open Source CFD Toolbox - User's Guide*. OpenCFD Ltd., United Kingdom, 2.3 edition.

[7] Formaggia, L., Miglio, E., Mola, A., and Parolini, N. Fluid-structure interaction problems in free surface flows: application to boat dynamics. *Int. J. Numer. Meth. Fluids*, (2008) **56**(8):965-978.

[8] Formaggia, L., Miglio, E., Mola, A., and Montano, A. A model for the dynamics of rowing boats. *Int. J. Numer. Meth. Fluids*, (2009) **61**(2): 119-143.

[9] Formaggia, L., Mola, A., Parolini, N., and Pischiutta, M. A three-dimensional model for the dynamics and hydrodynamics of rowing boats. *Proc. Inst. Mech. Eng., Part P: J. Sports Eng. Technol.*, (2010) **224**(1):51-61.

[10] *http://www.metoffice.gov.uk/news/in-depth/olympic-venue-weather/eton-dorney*